energy&fuels

pubs.acs.org/EF

Article

Experimental and Simulation Study for the Dissociation Behavior of Gas Hydrates – Part I: CH_4 Hydrates

Parisa Naeiji,* Mengdi Pan, Manja Luzi-Helbing, Saman Alavi, and Judith M. Schicks

Cite This: *Energy Fuels* 2023, 37, 4484–4496

Read Online

ACCESS | Metrics & More | Article Recommendations | Supporting Information

ABSTRACT: A study of methane hydrate dissociation under different temperature and pressure conditions combining *in situ* and *ex situ* Raman spectroscopic measurements, confocal microscopic characterizations, powder X-ray diffraction measurements, and molecular dynamics simulations was conducted. Both the experimental and the simulated data show that a distinction must be made between the dissociation behavior above and below the freezing point of water. During the dissociation process at temperatures near or below the freezing point of water, the simple CH_4 hydrates showed well-known self-preservation behaviors. The formation of a quasi-liquid or amorphous phase due to the decompositions of the hydrate cavities at the outer layers of the hydrate crystal terminated the further decomposition of the hydrate phase. For a CH_4 hydrate above the ice point, the dissociation appeared to be initiated at the surface of the hydrate phase. While significant amounts of the hydrate phase were present, the ratio of methane guests in the large and small cages remained constant. After large amounts of the hydrate phase decomposed, potential fragmentation of the remaining hydrate phase into collections of hydrate cages, which resulted in the preferred breakup of the tetrakaidecahedra ($5^{12}6^2$), was over the pentagonal dodecahedra (5^{12}).

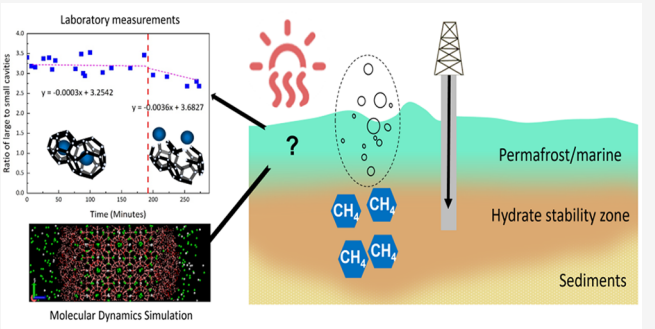

1. INTRODUCTION

Gas hydrates are ice-like crystalline solids in which water molecules trap gas molecules in clathrate structures.[1] Gas hydrates are stable under low-temperature and elevated-pressure conditions as can be found at continental margins, permafrost areas, and deep lakes.[2] Considering the huge amount of CH_4 enclathrated into natural gas hydrates and their worldwide distribution, an increasing awareness of the significance of CH_4 release from destabilized gas hydrate deposits occurred during the past decades.[3] An assessment from the Intergovernmental Panel on Climate Change (IPCC)[4] stated that CH_4 is deemed as a powerful greenhouses gas with a 100-year global warming potential of 28−34 times that of CO_2 and a 20-year global warming potential of 84−86 times that of CO_2. Thus, the release of CH_4 into the atmosphere from hydrate deposits would be of great concern. Methane release from hydrate deposits has been invoked as a contributing agent to the rapid warming events in geological times such as the Paleocene−Eocene Thermal Maximum[5] and Quaternary glacial-to-interglacial transitions.[6]

In turn, an increase in atmospheric temperature may induce hydrate dissociation, leading to the release of CH_4 from hydrate-bearing sediments. The gas hydrate destabilization might explain a large part of the atmospheric methane concentration oscillations that were recorded in polar ice cores during the last glacial episode.[7,8] Another effect on oceanic hydrates at continental margins is that sea level increases with rising temperature due to the melting of ice sheets lead to an increase in the overlying water column pressure, which partially counterbalances the potential threats of gas emission from hydrate dissociation due to increasing temperature.[9] Nevertheless, the stability of oceanic hydrates is still considered as a slow tipping point in the carbon cycle.[10] Evidence from the upper continental slope of Svalbard already suggested that the hydrate reservoirs in the Arctic were actively destabilized.[11] Permafrost hydrates, especially those associated within or beneath shallow permafrost layers, are more vulnerable to climate changes. Chuvilin et al.[12] investigated the effects of temperature increase on the frozen sediments containing metastable CH_4 hydrates in the sediment pores. The results indicated that even minor temperature increases (−3.0 to −0.3 °C, depending on lithology and salinity of the hosting sediments) can trigger large-scale dissociation of intrapermafrost hydrates. In addition, an assumption was made that the metastable gas hydrate could exist for a long period based on field and laboratory data due to the generated

Received: November 24, 2022
Revised: February 9, 2023
Published: February 23, 2023

ice film which covers the hydrate surface. This was introduced as self-preservation phenomena which play a crucial role in the kinetics of hydrate dissociation, so that the gas hydrate may partly convert to ice and back in a zone of recrystallization at the ice−hydrate boundary.[13−15] Considering the environmental effects, a proper understanding of CH_4 hydrate dissociation behavior with respect to climate change is urgently needed for an appropriate evaluation of the stabilities of natural gas hydrate deposits.

Gas hydrates formed from CH_4 are usually structure I hydrates, having two small 5^{12} cavities (pentagonal dodecahedra) and six large $5^{12}6^2$ cavities (tetrakaidecahedra).[16] Gupta et al.[17] provided time-resolved NMR results on CH_4 hydrate dissociation in which a constant cavity occupancy ratio throughout the process was observed. Liu et al.[18] also reported similar phenomenon from Raman spectroscopic data, implying that the sI unit cell decomposed as a single entity. This hypothesis was supported by some other researches.[19−23] However, the dissociation mechanism seems to be controversial, because a recent study from Truong-Lam et al.[24] suggested a preferential dissociation of the large $5^{12}6^2$ cavities.

To better understand the phenomena involved in the dissociation of gas hydrates, molecular dynamics (MD) simulations have also been conducted by several research groups.[25−32] They reported findings regarding the dissociation mechanism, rate, and effects of guests on the dissociation process. The first stage of the hydrate dissociation process was found to be associated with the diffusive behavior of water molecules and gas molecules escaping from the broken cavities.[28,30] English et al. indicated that the diffusion of CH_4 molecules to the surrounding liquid layer from the crystal surface appears to be the rate-controlling stage in the hydrate dissociation process which occurred at temperatures between 276.65 and 293 K and a pressure of 6.8 MPa.[33] Myshakin et al. observed no significant changes in the ratio of small (5^{12}) to large ($5^{12}6^2$) cavities during the first nanoseconds of the dissociation process but demonstrated oscillating behavior thereafter. This was attributed to reversible regrowth occurring at the interface and nucleating the water molecules around CH_4 molecules in the liquid phase, thereby forming partial hydrate cavities.[31] In these simulations, the hydrate phase decomposed in a concerted layer-by-layer manner, parallel to the sI cubic (100) surface, and the outermost layer of the decomposing hydrate participated in hydrate dissociation reformation.[25,34,35]

In this study, laboratory experiments simulated the dissociation process of simple structure I CH_4 hydrates applying *ex situ* and *in situ* Raman spectroscopy and *in situ* powder X-ray diffraction measurements together with confocal microscope observations. The dissociation process was based on thermal conduction and depressurization. As a supplement, molecular dynamics simulations on the dissociation process of CH_4 hydrate were conducted. Molecular dynamics simulations are on much smaller time and space scales than the experimental measurements, but they provide microscopic insight on some of the details of the phenomena and experimental observations. This study integrated Raman spectroscopic and X-ray diffraction measurements on a micrometer level and modeling efforts to better define the dissociation behavior of CH_4 hydrates. To our knowledge, there is a lack of such an integrated investigation involving both experiments and modeling at microscales and nanoscales. Our study filled the gap in this topic and quantified the time-dependent processes during CH_4 hydrate dissociation, which is among others essential for the estimation of possible CH_4 release from destabilization of natural gas hydrate reservoirs in response to global warming.

2. METHODOLOGY

2.1. Experimental Apparatus. Raman spectroscopic measurements were performed using a LabRAM HR Evolution dispersive Raman spectrometer from Horiba Scientific with 1800 grooves/mm grating coupled to an open microscope Olympus BX-FM. A 20× objective was selected for *in situ* Raman measurements, whereas a 50× objective was used for *ex situ* measurements. The excitation source was a frequency-doubled Nd:YAG solid-state laser with an output power of 100 mW working at 532 nm. With a focal length of 800 mm, this spectrometer achieves a maximum spectral resolution of 0.5 cm^{-1}. In order to verify the spectral resolution, a Raman spectrum of neon light was recorded, and the full width at half-maximum of the neon band at 1706 cm^{-1} was determined, from which a spectral resolution of 0.6 cm^{-1} resulted. A motorized pinhole in the analyzing beam path enables one to variably increase the spatial resolutions of laser-spot measurements which reach ∼0.5 μm in $x-y$ directions and ∼1.5 μm in the z direction at a maximum. During the measurements, the pinhole size was defined at 100 μm for *in situ* Raman measurements and 1000 μm for *ex situ* measurements, which offered the best spatial resolutions under specific conditions. In order to obtain a better signal-to-noise ratio for the Raman spectra, acquisition times of 5 s and two average exposures were chosen for the measurements. A silicon Raman band at 521 cm^{-1} was employed for the calibration of the Raman band positions before each experiment.

Time-dependent powder X-ray diffraction (PXRD) measurements were performed with a low-temperature−high-pressure cell that was integrated into a Bruker AXS Discover diffractometer with Cu Kα radiation generated at 40 kV and 40 mA. The pressure cell is running with a continuous gas flow ensuring a constant composition of the gas phase during the complete experiment. The cell can be operated in a pressure range between 0.1 and 4.0 MPa and in a temperature range between 253 and 288 K. The detection of the diffracted X-rays is carried out with GADDS (General Area Detection Diffraction System), which includes a HI-STAR area detector. Details of the low-temperature−high-pressure cell design, diffractometer, and experimental procedures for PXRD measurements are available elsewhere.[36,37]

2.2. Raman Spectroscopic Measurements. *2.2.1. In Situ.* *In situ* experiments were carried out in a custom-made high-pressure cell with a volume of 550 μL which can be integrated to a motorized, software-controlled Märzhauser Scan+ sample stage attached to the Raman system. To synthesize CH_4 hydrates, 150 μL of deionized water was loaded into the cell and pressurized with pure CH_4 gas at 7.0 MPa. The temperature of the cell was decreased to 253 K for the formation of ice and hydrates before it was maintained at 274 K (Figure 1). Due to the small volume of the cell and the complete cooling of the cell body by the Peltier element, temperature gradients can be neglected. Once sI CH_4 hydrate crystals were well developed, the temperature of the system was increased stepwise (277, 278, 279, 280, 280.5, 281, 281.5, 282, 282.5, and 283 K) to go across the equilibrium curve for hydrate decomposition. Since the increase of the system temperature and thus achieving thermal equilibrium may take

https://doi.org/10.1021/acs.energyfuels.2c03984
Energy Fuels 2023, 37, 4484−4496

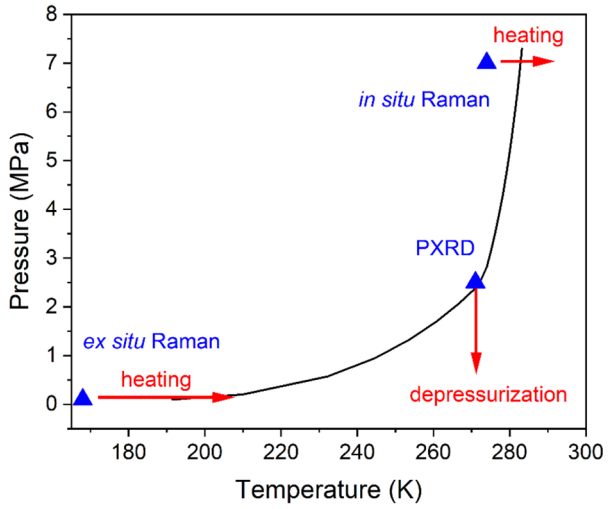

Figure 1. Experimental conditions for the *in situ* and *ex situ* measurements and the corresponding equilibrium curves calculated from the software CSMGem for pure CH_4 hydrates.[16] The starting condition (blue triangles) for the dissociation process was 7.0 MPa and 274 K for *in situ* Raman measurements and 0.1 MPa and 168 K for *ex situ* measurements. For the PXRD measurements, the starting condition was at 2.5 MPa and 271 K. The system was depressurized to 1.3 MPa.

some time, each temperature gradient was maintained for at least 20 min. During this period, the compositions of the selected hydrate crystals were measured. The collapse of hydrate structures can be sudden; hence, smaller steps (0.5 K) were made when the temperature approached the equilibrium curve. More details regarding the Raman spectroscopy, data analysis, and the pressure cell can be found elsewhere.[38]

2.2.2. Ex Situ. sI CH_4 hydrates were also formed from ice and CH_4 gas in batch pressure vessels with a volume of 420 mL. The formation of hydrates started with the preparation of ice by spraying deionized water into the liquid nitrogen bath. Ice beads were powdered by a pestle driven by a cryomagnet in a Spex 6750 Freezer Mill for 120 s, achieving a size range of 10−20 μm. Thereafter, the vessels loaded with the ice powder were sealed, pressurized at 7 MPa, and subsequently stored in a cooling box with the temperature fluctuating between 263 and 268 K for several weeks while monitoring the pressure drop. When there were no further changes in the pressure, CH_4 gas hydrate samples were recovered and quenched into liquid nitrogen. For further analysis with *ex situ* Raman spectroscopy, the recovered hydrate samples were quickly placed into a Linkam cooling stage at ambient pressure and 168 K. Single Raman spectra were collected continuously using the aforementioned confocal Raman spectrometer. The temperature of the system was increased by 1 K every 4−5 min. When there was a clear signal from either the spectrum or the microscopic observation indicating the start of the dissociation process, the temperature was maintained. The continuous Raman spectroscopic measurements ended when the hydrate signals disappeared from the spectra. The *ex situ* Raman measurements were repeated three times. Figure 1 depicts the p-T conditions for laboratory experiments. Raman spectroscopic data are available through GFZ Data Services.[39]

2.3. Powder X-ray Diffraction (PXRD) Measurements. Structure I CH_4 hydrate was first synthesized from hexagonal ice powder, which was generated in the same way as described for the *ex situ* Raman measurements. By means of scanning electron microscopy, the diameters of these ice particles were measured to about 10 μm.[40] At the next step, the precooled sample cell was filled with approximately 150 μL of powdered ice, carefully sealed, and mounted on the XYZ stage of the diffractometer. Thereafter, the sample cell was pressurized with CH_4 gas at 2.5 MPa and 264 K. Since the pressure cell was running with a continuous gas flow, a constant gas phase pressure was provided during the whole experiment. Respective crystal planes can be identified from the X-ray powder pattern which allows one to distinguish between the ice and the hydrate phase.[43] After a complete conversion of ice into hydrate, the temperature was increased to 271 K. To ensure that the ice is completely converted to hydrate, the temperature in the cell was raised slightly above the freezing point of ice. As soon as no more ice reflections could be recorded, the temperature and pressure were adjusted to the experimental conditions. Thereafter, the pressure was decreased to 50% below the stability limit at 271 K to 1.3 MPa (Figure 1). The dissociation process was monitored by continuously recording the powder pattern at five defined measuring points on the sample surface in the pressure cell. More detailed information is given elsewhere.[36,40]

The present phases were quantified by means of Rietveld refinement. For this purpose, the full pattern Rietveld program AutoQuan v2.7.1.0 was used.[41] The crystallographic data for structure I hydrate and ice data needed to create the structure model were obtained from the literature.[42−44] The refinement parameters were the phase fractions of ice and sI hydrate, seven background parameters, and lattice constants. The atomic positions and displacement parameters were fixed.

2.4. Molecular Dynamics Simulations. The GROMACS program (version 2018.8) was used to perform the molecular dynamics simulations.[45] The dissociation process was studied using a 3 × 3 × 6 unit cell replica of the structure I CH_4 hydrate with a dimension of 3.64 nm × 3.64 nm × 7.11 nm. The initial coordinates of the atoms of the water molecules in the unit cells are from the work of Takeuchi et al.[46] A row of water and CH_4 molecules were eliminated from one end of the hydrate phase in the z direction to get the hydrate phase symmetric along this direction. All hydrate cavities were occupied by CH_4 molecules. Figure 2 shows the initial configuration of the methane hydrate phase in the simulation box. The phase changes in the hydrate simulation appear to be localized in narrow layers of the hydrate phase and are stepwise

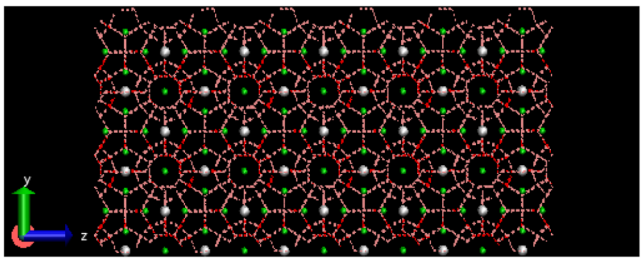

Figure 2. Initial configuration of the simulation box used in this work; a 3 × 3 × 6 slab of sI CH_4 hydrates with free (100) surfaces in the z direction. The hydrogen bonded water network in the clathrate hydrate is shown by the red lines. CH_4 molecules in the small and large cavities are shown by white and green spheres, respectively. Each hydrate cavity was occupied by only one CH_4 molecule.

https://doi.org/10.1021/acs.energyfuels.2c03984
Energy Fuels 2023, 37, 4484−4496

in time. Therefore, a finite hydrate sample can be an acceptable model for what happens in the bulk hydrate phase dissociation.

The hydrate phase was placed in the center of a simulation box (of around 3.64 nm × 3.64 nm × 10 nm) with vacuum on each side of the hydrate in the z direction to provide free interfaces at the (100) plane on which the heterogeneous decomposition was initiated. The (100) plane appears to be the most energetically stable surface in equilibrium contact even with the liquid phase.[25,33,34] Periodic boundary conditions were used in all three directions.

The intermolecular interactions of water molecules were modeled with the TIP4P/Ice model,[47] and CH_4 molecules were represented by the transferrable potentials for phase equilibria (TraPPE) united-atom (UA) potential.[48] The internal structures of the water molecules were kept rigid by using the LINCS algorithm.[49] The force field parameters are given in Table 1. All cross-interaction parameters between

Table 1. Force Field Parameters for Water (TIP4P/ice)[47] and CH_4 (TraPPE-UA)[48] Used in This Work

Atom	σ (nm)	ε (kcal·mol^{-1})	q (e)
O (H_2O)	0.3167	0.2108	0.0000
H (H_2O)			0.5897
M (H_2O)			−1.1794
C (CH_4)	0.3730	0.2941	0.0000

atoms on different molecules were determined using the Lorentz−Berthelot combining rules.[50] The Particle Mesh Ewald method[51,52] was used to evaluate the electrostatic interactions with a relative error of 10^{-6}. The cutoff of 1.4 nm was used for the short-range potentials.

The temperature and pressure of the simulation were maintained constant using a Berendsen thermostat and barostat[53] by the NPT ensemble. The equations of motion were integrated using the Leap-frog algorithm[54] with a time step of 2 fs.

The hydrate dissociation was implemented in simulations with simulation runs starting both below and above the ice point. For simulations above the ice point, the decomposition of the sI CH_4 hydrate system was simulated at a starting temperature of 274 K and pressure of 7.0 MPa. The temperature of the system increased stepwise until the dissociation of the hydrate phase was complete, following a procedure parallel to the *in situ* Raman experiments. The final temperature and pressure in this run were 318 K and 7.0 MPa. The stepwise change in temperature of the system with simulation time is shown in Figure S1 of the Supporting Information. The simulation below the ice point was performed at a temperature of 271 K, so that the starting pressure was 2.5 MPa at the first stage, and afterward, it was dropped to 1.3 MPa, which was identical to the experimental condition below the ice point for the PXRD measurements. The temperature and pressure profiles of the system with simulation time are given in Figure S2 of the Supporting Information.

There are criteria for quantitatively characterizing the dissociation process. The F_3 order parameter can be used for quantifying the local arrangement of water molecules in the hydrate and water phases[34] and is defined as

$$F_{3.i} = \langle [\cos\theta_{jik}|\cos\theta_{jik}| + \cos^2 109.47]^2 \rangle_{j.k} = \left\{ \begin{array}{c} 0.1 \text{ liquid water} \\ 0.0 \text{ solid water (ice, hydrate)} \end{array} \right\} \quad (1)$$

where atom i is in the center of a spherical shell of 0.35 nm including atoms j and k, and θ_{jik} shows the angle between three oxygen atoms of j, i, and k water molecules. The F_3 order parameter is around zero for water molecules in highly tetrahedral structures like ice and clathrate hydrate, and its value increases to ∼0.1 for liquid water. When the hydrate crystal is dissociated during the simulation trajectory, the F_3 parameter gradually increases. To quantify the spatial extent and progression of the hydrate dissociation, the initial hydrate phase was divided into the different layers parallel to the z direction (see Figures 10 and 13), and the F_3 parameter was calculated separately for each layer. Numerical simulation data are available through GFZ data services.[55]

3. RESULTS AND DISCUSSION

3.1. Raman Spectroscopic Measurements. Continuous *in situ* Raman spectroscopic measurements recorded changes in the hydrate phase upon heating. Two Raman bands at 2905 and 2915 cm^{-1} appeared in the Raman spectra while focusing the laser on the surface of the solid phase (Figure 3a). The Raman band at 2905 cm^{-1} is assigned to C−H stretching modes of CH_4 encapsulated into the large cavities ($5^{12}6^2$) of

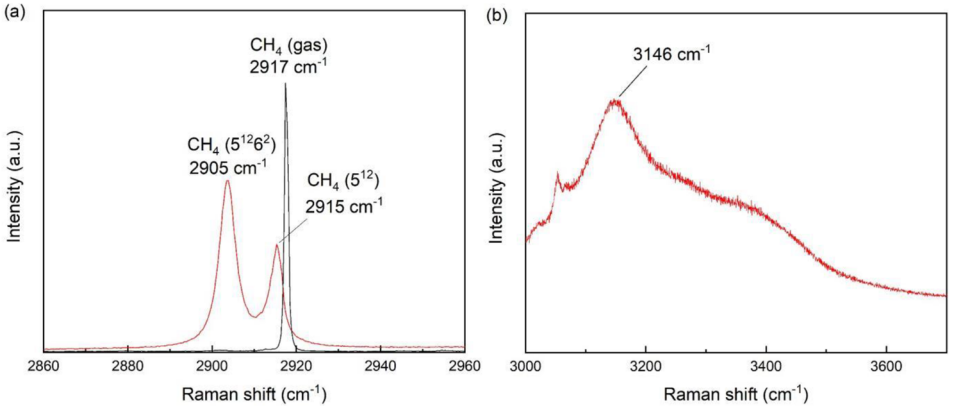

Figure 3. (a) Raman spectrum in red shows one signal for the CH_4 molecule encased into the large ($5^{12}6^2$) cavities at 2905 cm^{-1} and another band at 2915 cm^{-1}, representing a CH_4 molecule encased into the small (5^{12}) cavities of sI hydrates. The black Raman spectrum shows a prominent band for CH_4 at 2917 cm^{-1} in the gas phase. (b) O−H stretching modes ranged from 3000 to 3700 cm^{-1} for CH_4 hydrates.

https://doi.org/10.1021/acs.energyfuels.2c03984
Energy Fuels 2023, 37, 4484−4496

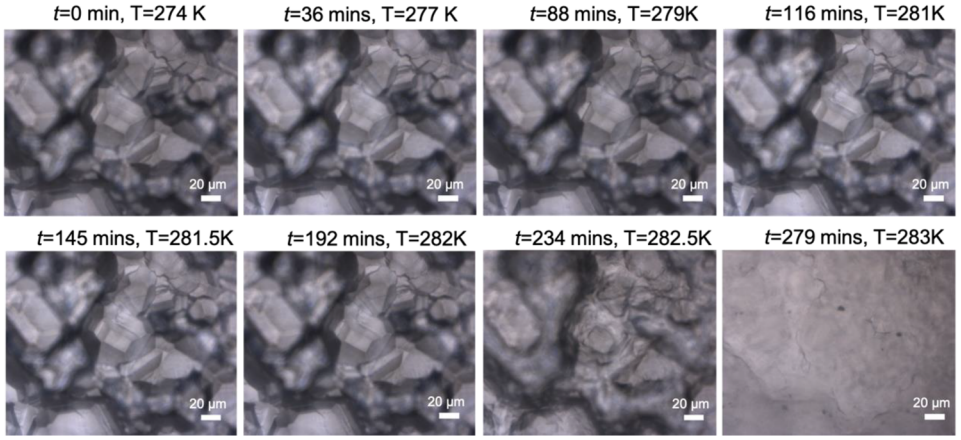

Figure 4. Microscopic images of CH_4 hydrate dissociation from *in situ* Raman measurements with increasing temperature at 7.0 MPa.

structure I hydrates, while the Raman band at 2915 cm^{-1} is assigned to C−H stretching modes of CH_4 encapsulated into the small cavities (5^{12}) of the structure I hydrate phase. With the continuous gas flow in the system, a narrow Raman band at 2917 cm^{-1} was also detected, which could be assigned to C−H stretching modes of CH_4 in the gas phase. As for the O−H stretching vibration between 3000 and 3500 cm^{-1}, a broad Raman band was observed at around 3146 cm^{-1} (Figure 3b), which corresponded to hydrogen bonds due to the formation of a well-structured hydrogen-bonded network in the hydrate phase.[56]

The confocal microscope coupled with a digital camera offered a unique opportunity for micrometer-scale visualization during *in situ* dissociation process. As displayed in Figure 4, well-developed micrometer-scale euhedral crystals were observed at 274 K, exhibiting polyhedral shapes with sharp edges and flat surfaces. Within the stability field of pure CH_4 hydrates, the morphologies of the crystals remained unchanged regardless of the increasing temperature. The crystals began to lose their original morphology at T = 282.5 K which was close to the equilibrium temperature (282.7 K, calculated from CSMGem) at 7.0 MPa, indicating that the dissociation was activated. All hydrate crystals subsequently decomposed at 283 K without any signs of self-preservation effects.

The Raman signals for the surrounding gas phase during *in situ* measurements of the hydrate phase were limited by the use of a confocal system; however, the presence of the signal from the gas could not be completely avoided. Since the Raman band for CH_4 gas (2917 cm^{-1}) is very close to that of CH_4 in the small (5^{12}) cavities (2915 cm^{-1}), the separation of these two Raman bands and thus the determination of the integrated intensities can become unreliable, especially at lower intensities of the Raman bands. However, exact values for the integrated intensities are necessary for the determination of the cavity occupancies. To avoid the influence of the gas phase, results from *ex situ* Raman measurements with no surrounding CH_4 gas phase were used for further analysis. Time-resolved *ex situ* Raman spectra recording the CH_4 hydrates dissociation process are shown in Figure 5. The results showed that both Raman band intensities for CH_4 in large ($5^{12}6^2$) and small (5^{12}) cavities started to decrease after 86 min, at a temperature of around 188 K, which was lower than the equilibrium temperature at ambient pressure as calculated from CSMGem (191.5 K).[16] The difference in dissociation temperature from the predicted CSMGem equilibrium value may be because the

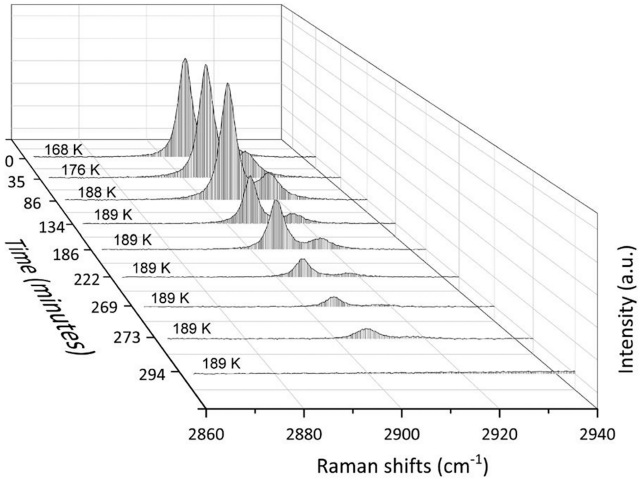

Figure 5. Real-time *ex situ* Raman spectra monitoring the dissociation process of CH_4 hydrates in the Linkam stage at ambient pressure.

hydrate system formed in the *ex situ* experiments did not reach an equilibrium state and may have a smaller absolute occupancy of the cavities, therefore less stable as compared to a hydrate phase with a higher cage occupancy. The Raman signals from the encapsulated CH_4 guests disappeared after 294 min where the temperature of the system was 189 K.

Correspondingly, these observations were consistent with the sequential images recorded during *ex situ* measurements in Figure 6 in which hydrate crystals either grew or maintained their shape within the first hour at atmospheric pressure where the temperature remained below 182 K. At around 188 K, in Figure 6, the flat crystal indicated by the red arrow split into several smaller crystals. The small crystals continued to shrink, while the hydrate crystals on the surface transformed into frost-like ice. Finally, the hydrate crystals totally converted to ice. Measurements taken at 15 and 30 μm depths only showed Raman signals for ice.

Figure 7 illustrates the changes of CH_4 occupancy in large ($5^{12}6^2$) and small (5^{12}) cavities for a specific hydrate crystal over time. Initially, the integrated Raman intensity of CH_4 in large ($5^{12}6^2$) and small (5^{12}) cavities approached or exceeds the theoretical value of 3:1,[57] indicating a higher percentage of large cavities ($5^{12}6^2$) being occupied with CH_4 compared to the occupancy of the small cavities (5^{12}). As shown in the figure, the ratio remained for around 186 min, as the

https://doi.org/10.1021/acs.energyfuels.2c03984
Energy Fuels 2023, 37, 4484−4496

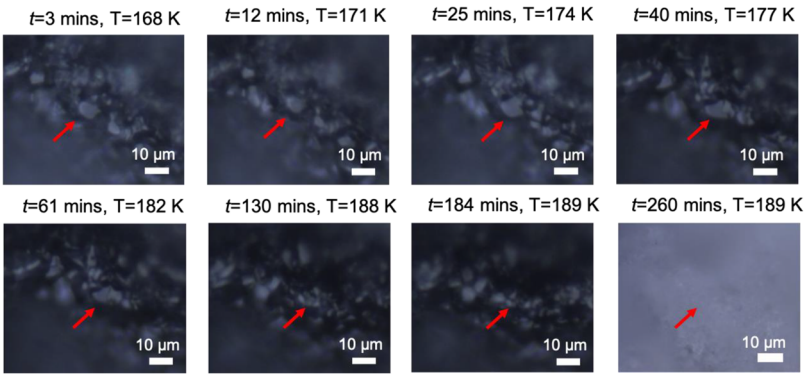

Figure 6. Microscopic observations of the pure CH_4 hydrates at atmospheric pressure with increasing temperature in the *ex situ* experiments. The red arrows marked the changes of the surface morphology of one specific crystal upon dissociation. The last panel indicates the breakup of the crystal.

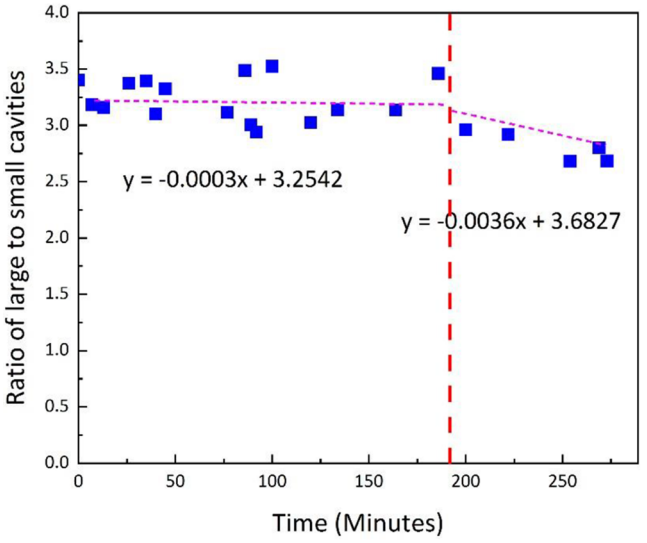

Figure 7. Ratio of large-to-small cavities as a function of time during the dissociation process of CH_4 hydrates based on the *ex situ* Raman measurements. The red dashed line indicates the turning point of the large-to-small cavity ratio which was at 210 K after 186 min.

temperature gradually increased to include temperatures above the hydrate equilibrium. This observation indicated that the hydrate dissociation retained the same ratio of large and small cavities during this period. After about 186 min, a slight decrease in the ratio of large-to-small cavities is observed, indicating that CH_4 molecules were released faster from the large $5^{12}6^2$ cavities compared to the release of CH_4 from small 5^{12} cavities. It was noteworthy that Raman signals for CH_4 in hydrate cavities were no longer detected after around 275 min indicating that all hydrates have been transformed into ice. The same phenomenon was also recorded when repeating the dissociation process (see Figure S3 of Supporting Information). However, the absolute duration time for the complete dissociation in each test varied.

3.2. Powder X-ray Diffraction Measurements. CH_4 hydrate was formed from ice at 2.5 MPa and 264 K. After a complete conversion of ice into hydrate as indicated by the XRD patterns, the temperature was increased to 271 K. At this temperature, the methane pressure was decreased to 50% below the equilibrium curve of the hydrate phase at given temperature. At 1.3 MPa, the powder patterns of five different spots on the sample surface were recorded at specified time steps. Due to significant changes in the sample morphology, the measurement of one sampling point had to be stopped during the measurement.

Figure 8 shows a fast dissociation of CH_4 hydrate within the first minutes of the experiment. The quantitative analysis of the

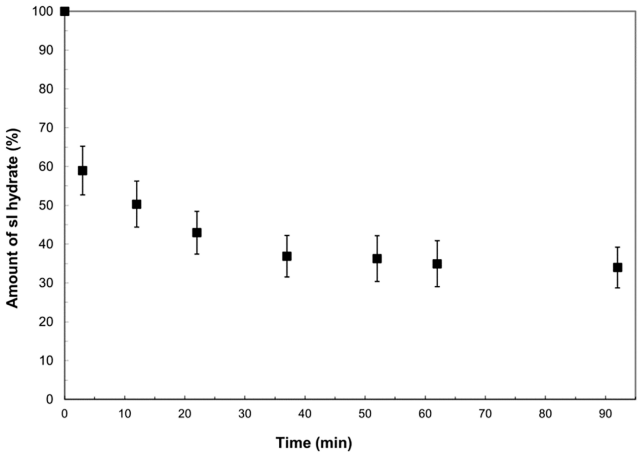

Figure 8. Percent of methane hydrate in a sample from a time-dependent PXRD experiment monitoring sI CH_4 hydrate dissociation at 271 K and 1.3 MPa.

powder patterns shows that within the first 5 min after pressure release approximately 40% of the sI hydrate is transformed into hexagonal ice. Subsequently, the amount of CH_4 hydrate stabilizes at ca. 35% ± 5% until the experiment was stopped after 90 min. This suggests the occurrence of the frequently described self-preservation effect of the hydrate which occurs below the ice point.[14]

3.3. MD Simulation of CH_4 Hydrate Dissociation. *3.3.1. Simulations above the Melting Point of Ice.* The MD simulations were performed to study the dissociation process of the structure I CH_4 hydrates at a starting pressure of 7.0 MPa and temperature of 274 K. The snapshots of the hydrate dissociation on the $y-z$ plane when the system was gradually heated are shown in Figure 9, so that the temperature at the final snapshot reached 318 K. The layered dissociation of the hydrate is observed in the direction parallel to the free hydrate interface, which in this case was the (100) surface. The hydrate phase started to dissociate from the outmost layers to the inner ones. A somewhat similar layer-by-layer dissociation mecha-

https://doi.org/10.1021/acs.energyfuels.2c03984
Energy Fuels 2023, 37, 4484−4496

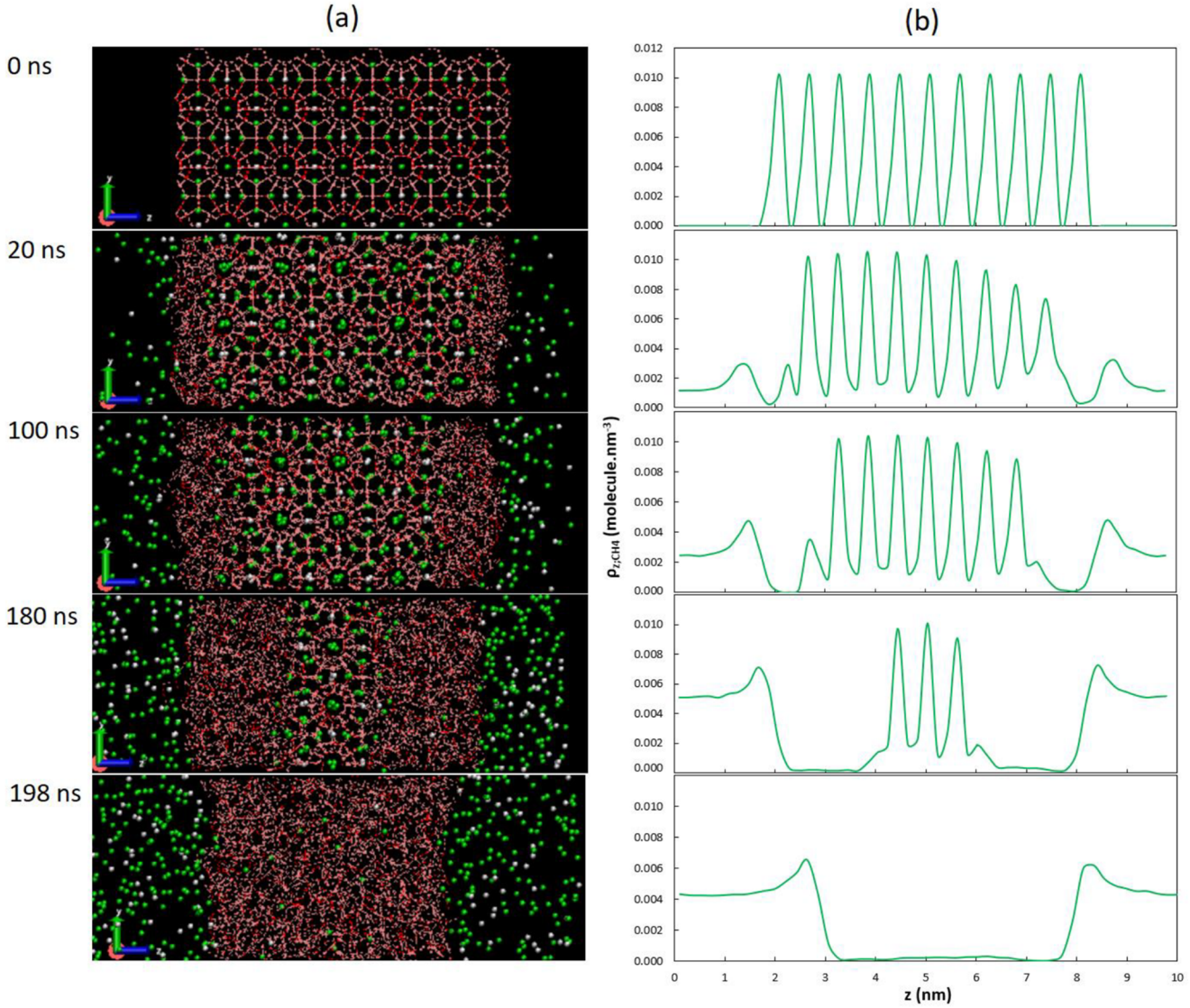

Figure 9. (a) Snapshots of CH_4 hydrate dissociation on the $y-z$ plane ((100) surface) at different times in the simulation trajectory. The temperature of the initial snapshot is at 274 K, and the temperature is increased stepwise as given in Figure S1 of the Supporting Information in such way that the final snapshot is at 318 K under the constant pressure of 7.0 MPa. The hydrogen bonding in the hydrate and liquid phase are shown by red lines. The CH_4 molecules in the small (5^{12}) and large ($5^{12}6^2$) cavities are represented by white and green spheres, respectively. Each hydrate cavity was occupied by only one CH_4 molecule. (b) The z density profile for CH_4 molecules during the dissociation process at corresponding times.

nism parallel to the interface has been observed for the sI CH_4 hydrates in previous simulations of CH_4 hydrate dissociation.[25,27,58,59] Incomplete open cavities promoted the decomposition of the hydrate structure at the interfaces, which led to the release of the encapsulated CH_4 molecules.

The z density profiles for all CH_4 molecules during the simulation are also shown in Figure 9. The periodic peaks in the initial configuration indicated the CH_4 molecules in the hydrate cavities. These peaks gradually disappeared from the two ends of the box as the dissociation proceeded. The fluid phases included both a liquid phase (water with a small number of dissolved CH_4 gas molecules) and free gas phase. At the gas−liquid interface, an excess CH_4 density was observed compared to the bulk gas phase that was a reflection of the wetting behavior of CH_4 on the water surface.[60] The CH_4 density at the gas phase increased as the dissociation proceeded. The animation from the trajectories of the simulation is given in the Supporting Information (Animation S1).

Details of the time evolution of hydrate dissociation can be further quantified by using the F_3 order parameter for different cross sections of the slab of the simulation cell parallel to the z direction. The time variation of F_3 for the different layers of the CH_4 hydrate upon increasing the temperature of the system is shown in Figure 10. At the starting temperature of 274 K, the outermost layers (with incomplete cavities) were partially decomposed as indicated by the increase of F_3 up to ∼0.03, implying that the water molecules in these layers were in a liquid-like amorphous phase. After around 10 ns, at the temperature of 281 K, layers 1 and 8 completely decomposed as their F_3 values reached around 0.07 and the inner layer of 2 and 7 started to dissociate. The temperature of 281 K is very

https://doi.org/10.1021/acs.energyfuels.2c03984
Energy Fuels 2023, 37, 4484−4496

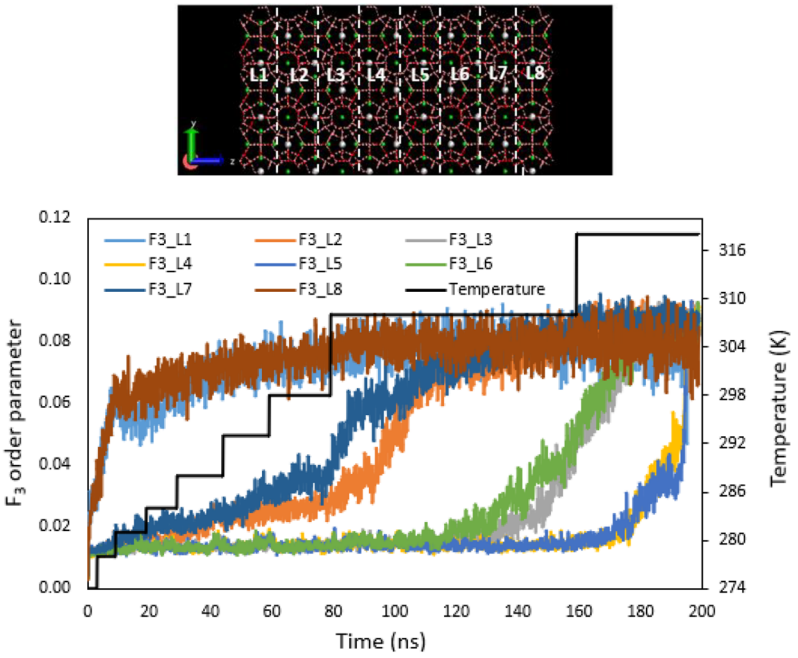

Figure 10. F_3 order parameter for layered CH_4 hydrate slab along the z direction for simulations above the ice point. As shown in the top panel, the hydrate phase was divided to the eight layers with layers 1 and 8 forming the outermost layers with incomplete cavities.

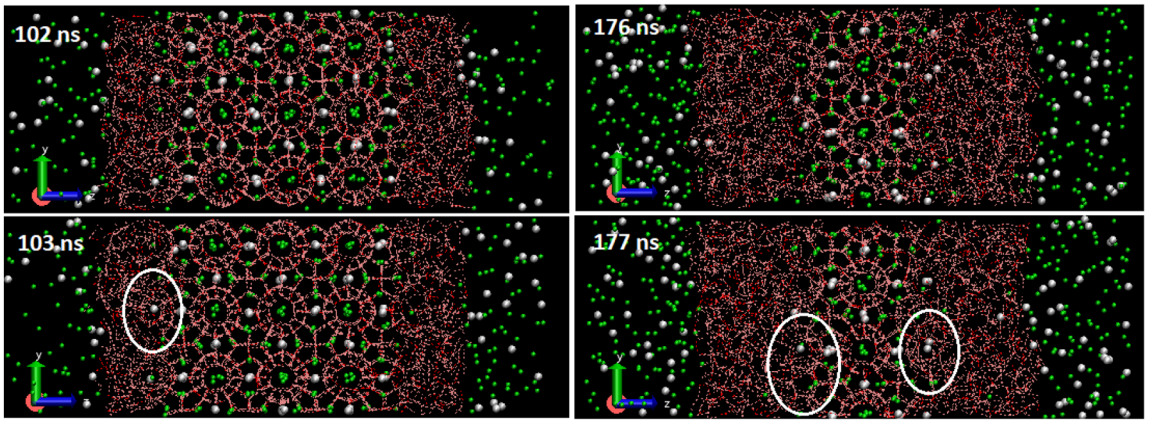

Figure 11. Snapshots of CH_4 hydrate dissociation simulation on the (100) surface showing the recrystallization of hydrate cavities during the dissociation process. The simulation temperature is above the ice point with the temperature profiles at different times given in Figure 10. White ovals show the recrystallized hydrate cavities.

close to the equilibrium temperature of the structure I CH_4 hydrate at this pressure; however, it is theoretically still within the stability field, as shown in Figure 1. Due to the details of the force fields used for water and CH_4, the hydrate structures used in the simulations may not dissociate at the same temperature as experimentally observed or calculated from the CSMGem software. Moreover, in the experiment, the hydrate phase may not reach an equilibrium state during the formation/dissociation process, and the small cages (5^{12}) of the CH_4 hydrate phase may not be fully occupied.

The melting of the outer layer of the clathrate phase resulted in the formation of an aqueous phase so that the dissociation of the inner layers and the gas diffusion slowed down. In addition, as seen in Figure 9, the concentration of CH_4 molecules in the vicinity of the hydrate surface increased which may induce locally an oversaturated aqueous phase. Water molecules may arrange around CH_4 molecules diffusing in the liquid phase, thereby forming or reforming partial hydrate cavities, as previously reported similarly in the related literature.[31,33] We tracked simulation snapshots and provide visual evidence for this phenomenon in Figure 11. These recrystallized partial hydrate cavities, as indicated by white ovals in Figure 11, are unstable and will disappear again after several time steps.

From Figure 10, the two first inner layers, 2 and 7, were totally decomposed after ~120 ns when the temperature conditions were above the equilibrium temperature at given pressure. Then, two other inner layers, 3 and 6, started to dissociate. Finally, at 318 K, the F_3 values of the last inner hydrate layers changed rapidly and approached to constant value of ~0.08 after approximately 200 ns. In this system, the dissociation of the hydrate was seen to occur in a sequential layer-by-layer manner. After an induction time, the outer layers decomposed on a relatively short time scale.

The main goal of the simulations was to understand if and how the ratio of occupied large ($5^{12}6^2$) to small (5^{12}) cavities changes during the dissociation of the CH_4 hydrates. This is

https://doi.org/10.1021/acs.energyfuels.2c03984
Energy Fuels 2023, 37, 4484−4496

the data compared to the experimental results shown in Figure 7. The ratio of large-to-small CH_4 guests was calculated according to the number of the released gas molecules during the process. Figure 12 shows the time variation of the ratio of

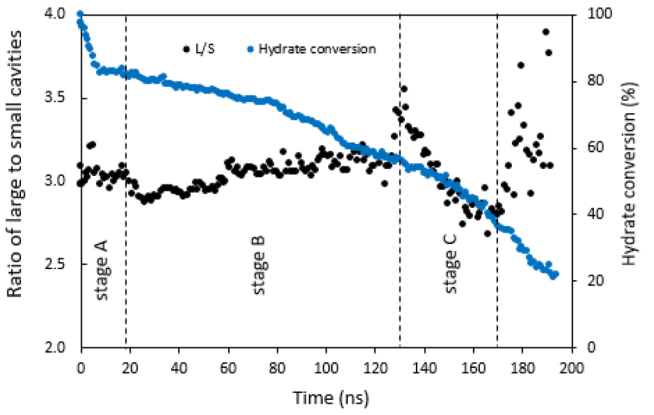

Figure 12. Ratio of large-to-small cavities and the hydrate conversion versus time for the sI CH_4 hydrate dissociation simulations above the ice point.

large-to-small CH_4 occupied cavities in the hydrate phase as well as the percent of hydrate conversion as a function of simulation time. The "hydrate conversion" was calculated by dividing the number of remaining hydrate cavities to the initial number of hydrate cavities as a percent, indicating the amount of gas hydrate converted to water and the gas phase. The results showed that at the beginning of hydrate dissociation, up to about 20 ns, the occupancy values scatter around a large-to-small cavity ratio of 3.0, which was consistent with the ratio of large-to-small cavities in the hydrate cell. This stage (stage A) corresponds to the decomposition of the two outermost layers, as shown in Figure 10. The ratio of large-to-small cavities increased between around 25 to 130 ns reaching up to a value of ~3.5 and fluctuated in the range of 3.0−3.5 implying that the CH_4 molecules occupying the small (5^{12}) cavities were released faster compared to those CH_4 molecules occupying the large ($5^{12}6^2$) cavities (stage B). Figure 10 shows that two first inner layers are dissociating at this stage. After ~130 ns, the partial decomposition of the next inner layers was observed, and it gradually proceeded for nearly 40 ns. This stage (stage C) is characterized by a significant decrease in the ratio of large-to-small cavities to values lower than 3. This indicates the breakup of the hydrate structure and large ($5^{12}6^2$) cavities releasing CH_4 molecules faster over this period. When the last layers of the hydrate cell were decomposing, the data scattered significantly which made it impossible to interpret a general trend.

Consistent with the experimental results shown in Figure 7, from the simulations, we observe that as long as large portions of the hydrate phase remain intact the ratio of CH_4 molecules in the large-to-small cages of the hydrate phase remains relatively stable. When the dissociation process proceeds, however, the ratio decreases, indicating a preferred release of CH_4 from large cavities.

As seen in Figure 12, in the beginning of the simulation, the hydrate conversion is high, and a large amount of CH_4 is released. Afterward, the hydrate conversion rate became slower. Thus, the release of CH_4 was slowed down or stopped, and the large-to-small cavity occupancy ratio remained stable subject to fluctuations during this period. During the end parts of the simulations and the experiments, perhaps due to the decomposition of the majority of the hydrate phase and its fragmentation to more amorphous collections of hydrate phases, the ratio of large-to-small cage methane molecules begins to change from the equilibrium value.

One reason for a possible better stabilization of the small (5^{12}) cavities by the inclusion of CH_4 molecules compared to the stabilization of the large ($5^{12}6^2$) cavities is the so-called

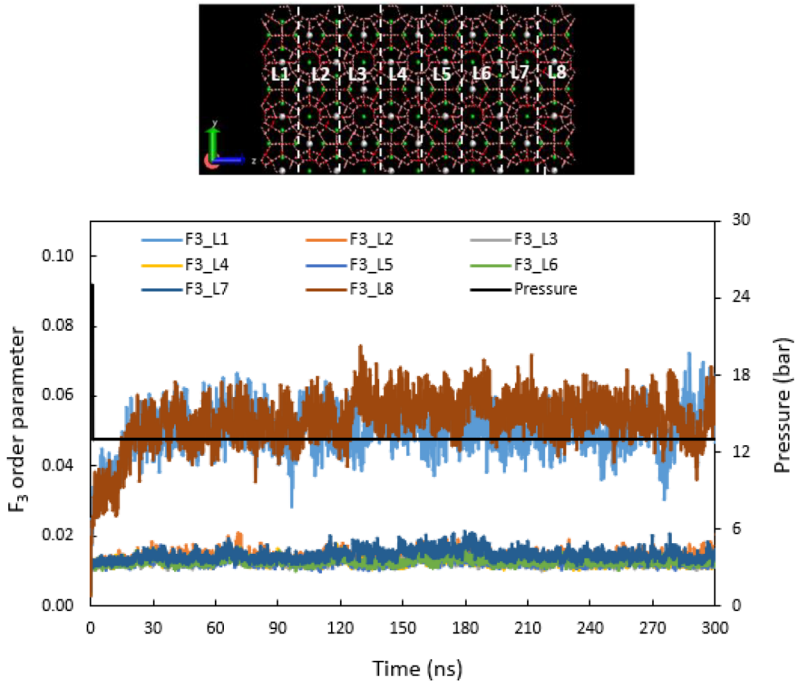

Figure 13. F_3 order parameter for layered CH_4 hydrate slab along the z direction for the simulation below the ice point at 271 K.

https://doi.org/10.1021/acs.energyfuels.2c03984
Energy Fuels 2023, 37, 4484−4496

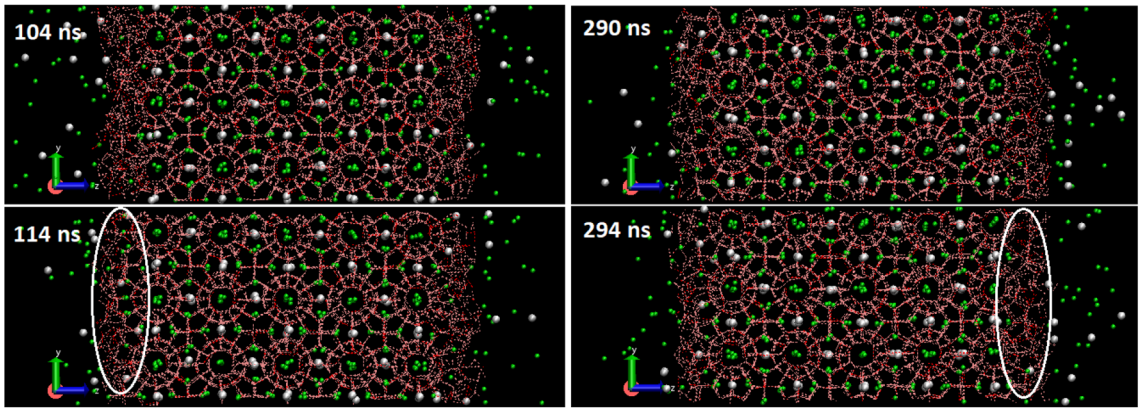

Figure 14. Snapshots of CH_4 hydrate simulation on the (100) surface showing the recrystallization of hydrate cavities or ice formation during the dissociation process at temperatures below the ice point. White ovals show the recrystallized hydrate cavities or ice formation.

guest-to-cavity ratio. Luzi-Helbing and Schicks calculated the van der Waals molecular diameter of 0.4018 nm for the CH_4 molecule.[37,61] The corresponding guest-to-cavity ratios for large $5^{12}6^2$ and small 5^{12} cavities are 0.69 and 0.79, respectively. According to Lederhos et al.,[62] a guest-to-cavity ratio between 0.75 and 1.0 results in an energy minimization and thus to a stabilization of the cavity structures. Apparently, these conditions are fulfilled only for CH_4 occupying the small 5^{12} cavities which indicates that CH_4 molecules are expected to better stabilize in isolated small 5^{12} cavities than large cavities. When the system is gradually heated up and hydrates are temporarily preserved outside the stability field, or hydrates begin to fragment into larger collections of cages, large $5^{12}6^2$ hydrate cavities rapidly collapse liberating CH_4 gas. Certainly, CH_4 in small cavities are also released in response to the breakup of neighboring cavities, but this process seems to be somewhat slower.

3.3.2. Simulations below the Melting Point of Ice. In these simulations, the CH_4 hydrate dissociation process was performed via the depressurization from 2.5 to 1.3 MPa at 271 K, according to the experimental conditions chosen for the X-ray diffraction measurements. An animation from the trajectories of the simulation is given in the Supporting Information (Animation S2). Figure 13 shows the F_3 order parameter for different cross sections of the slab of the simulation cell parallel to the z direction. The hydrate phase started to dissociate from the outermost layers to the inner ones similar to that observed in the previous simulation above the ice point. At the beginning, the F_3 value increased up to ~0.03 due to decomposing the incomplete cavities at the surface. After around 10 ns, layers 1 and 8 (the outmost layers) started to dissociate by increasing the F_3 values up to ~0.06, and they were completely decomposed after ~27 ns. The inner layers remained unchanged even after 300 ns of simulation time. Similar to the previous section, the ratio of large-to-small cavities during the dissociation of the CH_4 hydrates below the ice point was calculated and is given in Figure S4 of the Supporting Information. The results show that up to about 27 ns the hydrate cavities in the outer layers were broken up (see Figure 13) and the occupancy values scattered around a large-to-small cavity ratio of 3.0 characteristic of the hydrate phase as shown in Figure S4. Under these conditions, which are outside the hydrate stability zone, the hydrate breakup and the release of CH_4 molecules seem to have stopped.

Some visual hints on the observed behavior are shown in Figure 14. A quasi-liquid or amorphous aqueous phase appeared due to the hydrate breakup of the outer layers. As previously discussed, some unstable partial hydrate cavities were also formed which consequently resulted in the temporary slow down or stopping of gas release. Throughout the process, the hydrate undergoes decomposition−reformation processes. In addition, some new crystal structures, likely empty hydrate cavities or ice shells, were formed since the simulation was performed below the ice point (see Figure 14). According to the results, a self-preservation effect is assumed where the inner hydrate layers were mostly covered by ice or a dynamically slow amorphous water phase, which preserved the hydrates from the further dissociation. This is qualitatively consistent with the observations of Figure 8, which shows a self-preservation phenomenon for the real hydrate sample under these conditions.

4. SUMMARY AND CONCLUSIONS

In this work, a combination of laboratory Raman spectroscopic and powder X-ray diffraction measurements and molecular simulations was performed to investigate the dissociation behavior of sI CH_4 hydrates in response to p-T changes. The MD simulation results were in qualitative agreement with those obtained via the experiments. The main outcomes of the research are as follows:

- At the very early stages, in both experiments and simulations, the rate of hydrate dissociation was high. The ratio of CH_4 in large-to-small cavities in the hydrate phase was stabilized at around 3.0 which is consistent with the ratio of large ($5^{12}6^2$) and small (5^{12}) cavities in one unit cell.
- For temperatures above the ice point, the microscopic images and simulations indicate that dissociation is initiated at the surface of the hydrate phase and moves inward in the hydrate phase. During melting of the inner layers of hydrates, as long as sufficient hydrate was present, the large-to-small cavity occupancy ratio showed stable values with some fluctuations. By increasing the temperature, the ratio decreased upon the dissociation of inner layers and possible breakup of the remaining hydrate phase. During the last stages of the hydrate dissociation, the results confirmed that the breakup of large cavities was faster than those of the

https://doi.org/10.1021/acs.energyfuels.2c03984
Energy Fuels 2023, 37, 4484−4496

small ones. At subzero temperature and via depressurization, the recrystallization of the water molecules into hydrate-like structures or ice at the surface prevented further dissociation and inducing the well-known self-preservation effect for structure I CH_4 hydrate as was observed in the X-ray diffraction measurements.

- Neither during decomposition below nor above the ice point could a sudden dissociation of hydrate phase be observed. In the case of dissociation below the freezing point, the recrystallization of the water molecules into hydrate-like structures or ice at the surface prevented further dissociation. In the case of dissociation above the freezing point, the formation of an amorphous phase with partial cavity structures and local gas saturations led to a slowdown in hydrate decomposition.
- Confocal microscopic investigations during the Raman measurements showed the formation of a frost-like ice layer, which covered the crystals and was transformed from the original CH_4 hydrates. However, the self-preservation effects in *ex situ* Raman spectroscopic measurements were not recorded, since the applied conditions were out of the temperature zone for the occurrence of self-preservation effects.

On the basis of these comparable experiments and simulations, the dissociation process of sI CH_4 hydrates was visualized, providing insights on the fundamentals of the hydrate dissociation behavior at micrometer and nanometer scales. The knowledge of hydrate dissociation with regard to environmental changes may be useful in the assessment of CH_4 release to the atmosphere in nature from the dissociation of the hydrate phase. An extension of the present investigation addresses the dissociation process of structure II mixed gas hydrates (Part II of this work) which also frequently occur in natural reservoirs. This second study helped us to find the effect of structure and gas composition on the CH_4 release from destabilization hydrate reservoirs.

■ ASSOCIATED CONTENT

Data Availability Statement

Research data associated with this article can be accessed through GFZ data services: 10.5880/GFZ.3.1.2022.008 and 10.5880/GFZ.3.1.2022.007.

Supporting Information

The Supporting Information is available free of charge at https://pubs.acs.org/doi/10.1021/acs.energyfuels.2c03984.

Animation S1: Simulation trajectory of sI CH4 hydrate above the freezing point (MPG)

Animation S2: Simulation trajectory of sI CH4 hydrate below the freezing point (MPG)

Raman spectroscopic data from repeated tests and some MD outputs (PDF)

■ AUTHOR INFORMATION

Corresponding Author

Parisa Naeiji − *GFZ German Research Centre for Geosciences, 14473 Potsdam, Germany;* orcid.org/0000-0003-2206-5510; Email: parisa.naeiji@gfz-potsdam.de

Authors

Mengdi Pan − *GFZ German Research Centre for Geosciences, 14473 Potsdam, Germany; Key Laboratory of Gas Hydrate, Guangzhou Institute of Energy Conversion, Chinese Academy of Sciences, Guangzhou 510640, China; School of Chemical and Bioprocess Engineering, University College Dublin, Belfield, Dublin 4, Ireland*

Manja Luzi-Helbing − *GFZ German Research Centre for Geosciences, 14473 Potsdam, Germany*

Saman Alavi − *Department of Chemistry and Biomolecular Sciences, University of Ottawa, Ottawa, Ontario K1A 0R6, Canada;* orcid.org/0000-0001-9463-8766

Judith M. Schicks − *GFZ German Research Centre for Geosciences, 14473 Potsdam, Germany;* orcid.org/0000-0003-1106-0693

Complete contact information is available at: https://pubs.acs.org/10.1021/acs.energyfuels.2c03984

Author Contributions

Parisa Naeiji: conceptualization, numerical modeling investigation, writing − original draft, visualization. Mengdi Pan: conceptualization, experimental investigation (Raman spectroscopy), writing − original draft, visualization. Manja Luzi-Helbing: experimental investigation (PXRD), writing − review and editing. Saman Alavi: writing − review and editing. Judith Schicks: conceptualization, writing − review and editing, supervision. Parisa Naeiji and Mengdi Pan contributed equally to this work.

Notes

The authors declare no competing financial interest.

■ ACKNOWLEDGMENTS

The authors sincerely acknowledge Dr. Erik Spangenberg and Ronny Giese for their invaluable technical support during the experiments. Mengdi Pan appreciates the financial support from the Chinese Scholarship Council (201704910817) and the Open Fund Project of the Key Laboratory of Natural Gas Hydrate, Guangzhou Institute of Energy Conversion, Chinese Academy of Sciences (E129kf1401).

■ REFERENCES

(1) von Stackelberg, M. Feste Gashydrate. *Naturwissenschaften* **1949**, *36*, 327−333.

(2) Kvenvolden, K. A. Gas Hydrates—Geological Perspective and Global Change. *Rev. Geophys.* **1993**, *31* (2), 173−187.

(3) Ruppel, C. D.; Kessler, J. D. The Interaction of Climate Change and Methane Hydrates. *Rev. Geophys.* **2017**, *55* (1), 126−168.

(4) Intergovernmental Panel on Climate Change (IPCC). *Climate Change 2013: The Physical Science Basis. Contribution of Working Group I to the Fifth Assessment Report of the Intergovernmental Panel on Climate Change*; Cambridge University Press: Cambridge, UK and New York, 2013.

(5) Dickens, G. R.; O'Neil, J. R.; Rea, D. K.; Owen, R. M. Dissociation of Oceanic Methane Hydrate as a Cause of the Carbon Isotope Excursion at the End of the Paleocene. *Paleoceanography* **1995**, *10* (6), 965−971.

(6) Kennett, J. P.; Cannariato, K. G.; Hendy, C. H. *Methane Hydrates in Quaternary Climate Change: The Clathrate Gun Hypothesis*; American Geophysical Union: Washington DC, 2003.

(7) de Garidel-Thoron, T.; Beaufort, L.; Bassinot, F.; Henry, P. Evidence for Large Methane Releases to the Atmosphere from Deep-Sea Gas-Hydrate Dissociation during the Last Glacial Episode. *Proc. Natl. Acad. Sci. U. S. A.* **2004**, *101* (25), 9187−9192.

(8) Bock, J.; Martinerie, P.; Witrant, E.; Chappellaz, J. Atmospheric Impacts and Ice Core Imprints of a Methane Pulse from Clathrates. *Earth Planet. Sci. Lett.* **2012**, *349*−*350*, 98−108.

(9) Sultan, N.; Plaza-Faverola, A.; Vadakkepuliyambatta, S.; Buenz, S.; Knies, J. Impact of Tides and Sea-Level on Deep-Sea Arctic

Methane Emissions. *Nat. Commun.* **2020**, *11* (1). DOI: 10.1038/s41467-020-18899-3.
(10) Archer, D.; Buffett, B.; Brovkin, V. Ocean Methane Hydrates as a Slow Tripping Point in the Global Carbon Cycle. *Proc. Natl. Acad. Sci. U. S. A.* **2009**, *106* (49), 20596−20601.
(11) Westbrook, G. K.; Thatcher, K. E.; Rohling, E. J.; Piotrowski, A. M.; Pälike, H.; Osborne, A. H.; Nisbet, E. G.; Minshull, T. A.; Lanoisellé, M.; James, R. H.; Hühnerbach, V.; Green, D.; Fisher, R. E.; Crocker, A. J.; Chabert, A.; Bolton, C.; Beszczynska-Möller, A.; Berndt, C.; Aquilina, A. Escape of Methane Gas from the Seabed along the West Spitsbergen Continental Margin. *Geophys. Res. Lett.* **2009**, *36* (15), n/a.
(12) Chuvilin, E.; Davletshina, D.; Ekimova, V.; Bukhanov, B.; Shakhova, N.; Semiletov, I. Role of Warming in Destabilization of Intrapermafrost Gas Hydrates in the Arctic Shelf: Experimental Modeling. *Geosci.* **2019**, *9*, 407.
(13) Yershov, E. D.; Lebedenko, Y. P.; Chuvilin, Y. M.; Istomin, V. A.; Yakushev, V. S. The Problems of the Stability of Gas-Hydrate Deposits in the Cryolithozone. *Bull. Moscow Univ.* **1992**, *5* (4), 82−87.
(14) Istomin, V. A.; Yakushev, V. S.; Makhonina, N. A.; Kwon, V. G.; Chuvilin, E. M. Self-Preservation Phenomenon of Gas Hydrates. *Gas Ind. Russ.* **2006**, *4*, 16−27.
(15) Chuvilin, E.; Davletshina, D.; Bukhanov, B.; Mukhametdinova, A.; Istomin, V. Formation of Metastability of Pore Gas Hydrates in Frozen Sediments: Experimental Evidence. *Geosciences* **2022**, *12* (11), 419.
(16) Sloan, E. D.; Koh, C. A. *Clathrate Hydrates of Natural Gases*, 3rd ed.; CRC Press Taylor and Francis Group: Boca Raton, FL, USA, 2008.
(17) Gupta, A.; Dec, S. F.; Koh, C. A.; Sloan, E. D. NMR Investigation of Methane Hydrate Dissociation. *J. Phys. Chem. C* **2007**, *111*, 2341−2346.
(18) Liu, C.; Lu, H.; Ye, Y.; Ripmeester, J. A.; Zhang, X. Raman Spectroscopic Observations on the Structural Characteristics and Dissociation Behavior of Methane Hydrate Synthesized in Silica Sands with Various Sizes. *Energy Fuels* **2008**, *22*, 3986−3988.
(19) Rovetto, L. J.; Bowler, K. E.; Stadterman, L. L.; Dec, S. F.; Koh, C. A.; Sloan, E. D. Dissociation Studies of CH4-C2H6 and CH4-CO2 Binary Gas Hydrates. *Fluid Phase Equilib.* **2007**, *261* (1−2), 407−413.
(20) Zhou, X.; Long, Z.; Liang, S.; He, Y.; Yi, L.; Li, D.; Liang, D. In Situ Raman Analysis on the Dissociation Behavior of Mixed CH4-CO2 Hydrates. *Energy Fuels* **2016**, *30* (2), 1279−1286.
(21) Tang, C.; Zhou, X.; Li, D.; Zhao, X.; Liang, D. In Situ Raman Investigation on Mixed CH4 -C3H8 Hydrate Dissociation in the Presence of Polyvinylpyrrolidone. *Fuel* **2018**, *214*, 505−511.
(22) Dec, S. F.; Bowler, K. E.; Stadterman, L. L.; Koh, C. A.; Sloan, E. D. NMR Study of Methane + Ethane Structure I Hydrate Decomposition. *J. Phys. Chem. A* **2007**, *111* (20), 4297−4303.
(23) Zhong, J. R.; Zeng, X. Y.; Zhou, F. H.; Ran, Q. D.; Sun, C. Y.; Zhong, R. Q.; Yang, L. Y.; Chen, G. J.; Koh, C. A. Self-Preservation and Structural Transition of Gas Hydrates during Dissociation below the Ice Point: An in Situ Study Using Raman Spectroscopy. *Sci. Rep.* **2016**, *6*, 1−13.
(24) Truong-Lam, H. S.; Seo, S. D.; Kim, S.; Seo, Y.; Lee, J. D. In Situ Raman Study of the Formation and Dissociation Kinetics of Methane and Methane/Propane Hydrates. *Energy Fuels* **2020**, *34* (5), 6288−6297.
(25) Alavi, S.; Ripmeester, J. A. Nonequilibrium Adiabatic Molecular Dynamics Simulations of Methane Clathrate Hydrate Decomposition. *J. Chem. Phys.* **2010**, *132*, 144703.
(26) English, N. J.; MacElroy, J. M. D. Perspectives on Molecular Simulation of Clathrate Hydrates: Progress, Prospects and Challenges. *Chem. Eng. Sci.* **2015**, *121*, 133−156.
(27) Bagherzadeh, S. A.; Englezos, P.; Alavi, S.; Ripmeester, J. A. Molecular Simulation of Non-Equilibrium Methane Hydrate Decomposition Process. *J. Chem. Thermodyn.* **2012**, *44* (1), 13−19.
(28) Iwai, Y.; Nakamura, H.; Arai, Y.; Shimoyama, Y. Analysis of Dissociation Process for Gas Hydrates by Molecular Dynamics Simulation. *Mol. Simul.* **2010**, *36* (3), 246−253.
(29) Yagasaki, T.; Matsumoto, M.; Tanaka, H. Effects of Thermodynamic Inhibitors on the Dissociation of Methane Hydrate: A Molecular Dynamics Study. *Phys. Chem. Chem. Phys.* **2015**, *17* (48), 32347.
(30) Ding, L. Y.; Geng, C. Y.; Zhao, Y. H.; Wen, H. Molecular Dynamics Simulation on the Dissociation Process of Methane Hydrates. *Mol. Simul.* **2007**, *33* (12), 1005−1016.
(31) Myshakin, E. M.; Jiang, H.; Warzinski, R. P.; Jordan, K. D. Molecular Dynamics Simulations of Methane Hydrate Decomposition†. *J. Phys. Chem. A* **2009**, *113* (10), 1913−1921.
(32) Ji, H.; Chen, D.; Zhao, C.; Wu, G. Molecular Dynamics Simulation of Methane Hydrate Formation and Dissociation in the Clay Pores with Fatty Acids. *J. Phys. Chem. C* **2018**, *122* (2), 1318−1325.
(33) English, N. J.; Johnson, J. K.; Taylor, C. E. Molecular-Dynamics Simulations of Methane Hydrate Dissociation. *J. Chem. Phys.* **2005**, *123* (24), 244503.
(34) Báez, L. A.; Clancy, P. Computer Simulation of the Crystal Growth and Dissolution of Natural Gas Hydrates. *Ann. N.Y. Acad. Sci.* **1994**, *715* (1), 177−186.
(35) English, N. J.; Phelan, G. M. Molecular Dynamics Study of Thermal-Drivenmethane Hydrate Dissociation. *J. Chem. Phys.* **2009**, *131*, 074704.
(36) Luzi, M.; Girod, M.; Naumann, R.; Schicks, J. M.; Erzinger, J. A High-Pressure Cell for Kinetic Studies on Gas Hydrates by Powder x-Ray Diffraction. *Rev. Sci. Instrum.* **2010**, *81* (12), 125105.
(37) Luzi-Helbing, M. Kinetic Studies of Mixed Gas Hydrates. Thesis, GFZ, 2012.
(38) Schicks, J. M.; Pan, M.; Giese, R.; Poser, M.; Ismail, N. A.; Luzi-Helbing, M.; Bleisteiner, B.; Lenz, C. A New High-Pressure Cell for Systematic in Situ Investigations of Micro-Scale Processes in Gas Hydrates Using Confocal Micro-Raman Spectroscopy. *Rev. Sci. Instrum.* **2020**, *91* (11), 115103.
(39) Pan, M.; Schicks, J. M. *Raman Spectroscopic Data from Dissociation Behavior of SI CH4 Hydrates, SII CH4-C3H8 Hydrates and Multicomponent Mixed Gas Hydrates in Terms of Thermal Stimulation*; GFZ Data Services, 2022. https://doi.org/10.5880/GFZ.3.1.2022.008.
(40) Luzi, M.; Schicks, J. M.; Naumann, R.; Erzinger, J. Systematic Kinetic Studies on Mixed Gas Hydrates by Raman Spectroscopy and Powder X-Ray Diffraction. *J. Chem. Thermodyn.* **2012**, *48*, 28−35.
(41) Kleeberg, R.; Bergmann, J. Quantitative Röntgenphasenanalyse Mit Den Rietveld- Programmen BGMN Und AUTOQUANT in Der Täglichen Laborpraxis. *Berichte der DTTG e.V.* **1998**, *Band 6* (6), 237−250.
(42) Rundle, R. E. The Structure and Residual Entropy of Ice. *J. Chem. Phys.* **1953**, *21* (7), 1311.
(43) Yousuf, M.; Qadri, S. B.; Knies, D. L.; Grabowski, K. S.; Coffin, R. B.; Pohlman, J. W. Applied Physics A Novel Results on Structural Investigations of Natural Minerals of Clathrate Hydrates. *Appl. Phys. A: Mater. Sci. Process.* **2004**, *78*, 925−939.
(44) Kirchner, M. T.; Boese, R.; Billups, W. E.; Norman, L. R. Gas Hydrate Single-Crystal Structure Analyses. *J. Am. Chem. Soc.* **2004**, *126* (30), 9407−9412.
(45) Van Der Spoel, D.; Lindahl, E.; Hess, B.; Groenhof, G.; Mark, A. E.; Berendsen, H. J. C. GROMACS: Fast, Flexible, and Free. *J. Comput. Chem.* **2005**, *26* (16), 1701−1718.
(46) Takeuchi, F.; Hiratsuka, M.; Ohmura, R.; Alavi, S.; Sum, A. K.; Yasuoka, K. Water Proton Configurations in Structures I, II, and H Clathrate Hydrate Unit Cells. *J. Chem. Phys.* **2013**, *138* (12), 124504.
(47) Abascal, J. L. F.; Sanz, E.; Garcia Fernandez, R.; Vega, C. A Potential Model for the Study of Ices and Amorphous Water: TIP4P/Ice. *J. Chem. Phys.* **2005**, *122* (23), 234511.
(48) Martin, M. G.; Siepmann, J. I. Transferable Potentials for Phase Equilibria. 1. United-Atom Description of n-Alkanes. *J. Phys. Chem. B* **1998**, *102* (14), 2569−2577.

(49) Hess, B.; Bekker, H.; Berendsen, H. J. C.; Fraaije, J. G. E. M. LINCS: A Linear Constraint Solver for Molecular Simulations. *J. Comput. Chem.* **1997**, *18* (12), 1463−1472.
(50) Docherty, H.; Galindo, A.; Vega, C.; Sanz, E. A Potential Model for Methane in Water Describing Correctly the Solubility of the Gas and the Properties of the Methane Hydrate. *J. Chem. Phys.* **2006**, *125* (7), 074510.
(51) Alavi, S. *Molecular Simulations: Fundamentals and Practice*; Wiley-VCH Verlag GmbH: Weinheim, Germany, 2020; Vol. *1*.
(52) Darden, T.; York, D.; Pedersen, L. Particle Mesh Ewald: An N·log(N) Method for Ewald Sums in Large Systems. *J. Chem. Phys.* **1993**, *98*, 10089−10092.
(53) Berendsen, H. J. C.; Postma, J. P. M.; Van Gunsteren, W. F.; Dinola, A.; Haak, J. R. Molecular Dynamics with Coupling to an External Bath. *J. Chem. Phys.* **1984**, *81* (8), 3684−3690.
(54) Hockney, R. W.; Goel, S. P.; Eastwood, J. W. Quiet High-Resolution Computer Models of a Plasma. *J. Comput. Phys.* **1974**, *14* (2), 148−158.
(55) Naeiji, P.; Schicks, J. M. *Molecular Dynamics Simulation Data for Dissociation of CH4 and Mixed Gas Hydrates*; GFZ Data Services, 2022. https://doi.org/10.5880/GFZ.3.1.2022.007.
(56) Walrafen, G. E.; Yang, W. H.; Chu, Y. C. Raman Evidence for the Clathratelike Structure of Highly Supercooled Water. *ACS Symp. Ser.* **1997**, *676*, 287−308.
(57) Uchida, T.; Takeya, S.; Kamata, Y.; Ikeda, I. Y.; Nagao, J.; Ebinuma, T.; Narita, H.; Zatsepina, O.; Buffett, B. A. Spectroscopic Observations and Thermodynamic Calculations on Clathrate Hydrates of Mixed Gas Containing Methane and Ethane: Determination of Structure, Composition and Cage Occupancy. *J. Phys. Chem. B* **2002**, *106* (48), 12426−12431.
(58) Conde, M. M.; Vega, C. Determining the Three-Phase Coexistence Line in Methane Hydrates Using Computer Simulations. *J. Chem. Phys.* **2010**, *133* (6), 064507.
(59) Yan, K.; Li, X.; Chen, Z.; Li, B.; Xu, C. Molecular Dynamics Simulation of Methane Hydrate Dissociation by Depressurisation. *Mol. Simul.* **2013**, *39* (4), 251−260.
(60) Naeiji, P.; Woo, T. K.; Alavi, S.; Varaminian, F.; Ohmura, R. Interfacial Properties of Hydrocarbon/Water Systems Predicted by Molecular Dynamic Simulations. *J. Chem. Phys.* **2019**, *150* (11), 114703.
(61) Schicks, J. M.; Luzi-Helbing, M. Kinetic and Thermodynamic Aspects of Clathrate Hydrate Nucleation and Growth. *J. Chem. Eng. Data* **2015**, *60* (2), 269−277.
(62) Lederhos, J. P.; Christiansen, R. L.; Sloan, E. D. A First Order Method of Hydrate Equilibrium Estimation and Its Use with New Structures. *Fluid Phase Equilib.* **1993**, *83* (C), 445−454.

https://doi.org/10.1021/acs.energyfuels.2c03984
Energy Fuels 2023, 37, 4484−4496